[*Supporting Information*]

Observation of Interpenetration Isomerism in Covalent Organic Frameworks

Tianqiong Ma,[†,‡] Jian Li,[‡] Jing Niu,[†] Lei Zhang,[‡] Ahmed S. Etman,[§] Cong Lin,[‡] Dier Shi,[‡] Pohua Chen,[‡] Li-Hua Li,[†] Xin Du,[‡] Junliang Sun,*[,‡,§] and Wei Wang*[,†,¶]

[†]State Key Laboratory of Applied Organic Chemistry, College of Chemistry and Chemical Engineering, Lanzhou University, Lanzhou, Gansu 730000, China

[‡]College of Chemistry and Molecular Engineering, Beijing National Laboratory for Molecular Sciences, Peking University, Beijing 100871, China

[§]Department of Materials and Environmental Chemistry, Stockholm University, Stockholm 10691, Sweden

[¶]Collaborative Innovation Center of Chemical Science and Engineering, Tianjin 300071, China

*E-mail: junliang.sun@pku.edu.cn; wang_wei@lzu.edu.cn

Table of Contents

Summary of Schemes, Tables and Figures

A. Synthetic Procedures

All reagents and solvents, unless otherwise specified, were purchased from commercial sources and used without further purification. Monomer **1** was synthesized according to the reported procedures.[1] Meanwhile, following the reported procedure,[2] we were able to reproduce the synthesis of ***dia-c5*** COF-300, the phase purity of which has been verified by thorough characterization (see below). Most importantly, we found that an interpenetration isomer, ***dia-c7*** COF-300, could be reproducibly obtained upon changing the synthetic parameters (see below).
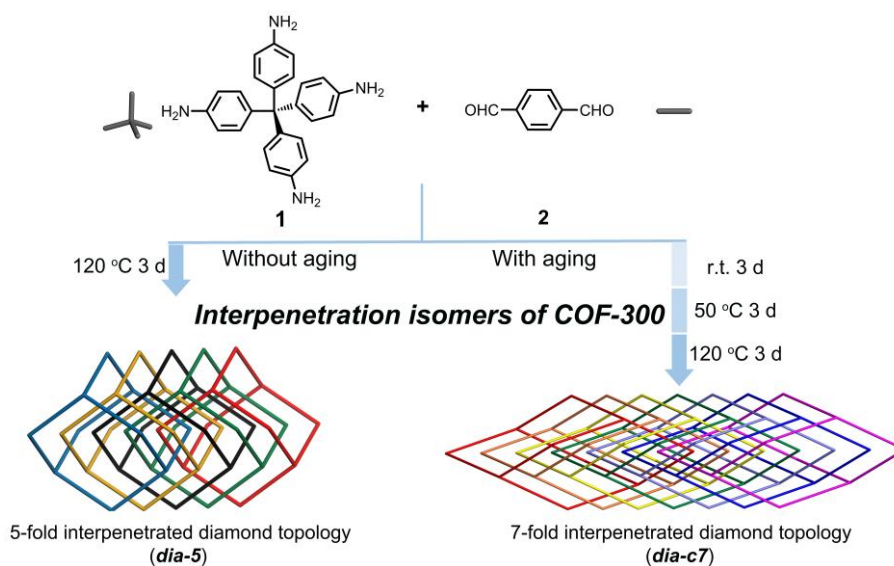
Scheme 1. Solvothermal condensation of **1** and **2** under different conditions resulted in two interpenetration isomers of COF-300.

Typical procedure for the synthesis of *dia-c7* COF-300. A 10 mL glass tube was charged with tetra-(4-anilyl)methane **1** (20.0 mg, 0.052 mmol), terephthaldehyde **2** (12.0 mg, 0.089 mmol), and 1.0 mL of 1,4-dioxane. Then 0.2 mL of aqueous acetic acid (6 M) was added into the solution. The tube was flash frozen in a liquid nitrogen bath, evacuated to vacuum and flame sealed. In difference from the reported procedure[2] for ***dia-c5*** COF-300, the fused tube was allowed to stand at room temperature for 72 h and then warmed at 50 °C for 72 h, which represents as an aging process. After aging, the fused tube was further heated at 120 °C for 72 h, the process of which is identical to that[2] for synthesizing ***dia-c5*** COF-300. During the aging process, an amorphous solid was obtained after aging the mixture at room temperature for 72 h. After keeping on warming the mixture at 50 °C for 72 h, a crystalline solid (***dia-c7*** COF-300 with a few

dia-c5 COF-300) was formed. The crystallinity can be improved after heating them at 120 °C, and *dia-c5* COF-300 may transform to *dia-c7* COF-300. Formed as a yellow solid, the crude product was isolated by centrifugation and Soxhlet extraction in 1,4-dioxane for 24 h, dried at ambient temperature for 12 h, and further dried at 120°C for 12 h to afford a yellow powder. Yield: 83.6% (21.4 mg) based on **2**. Elemental analysis: calcd for $C_{41}H_{28}N_4$: C 85.42%; H 4.86%; N 9.72%. Found: C 79.63%; H 4.21%; N 9.00%. As described in detail in the main text, this solid (denoted as *dia-c7* COF-300) was identified by PXRD and RED analyses as an interpenetration isomer of *dia-c5* COF-300. Similar to *dia-c5* COF-300, *dia-c7* COF-300 was insoluble in water and common organic solvents such as hexanes, methanol, acetone, tetrahydrofuran, and *N,N*-dimethylformamide.

Controllable synthesis of *dia-c5* and *dia-c7* COF-300 isomers. Orthogonal experiments were carried to systematically alter the reaction parameters (*e.g.* concentrations of the monomers and HOAc, reaction temperatures, aging conditions, and so on). The general procedure was described as follows. A 10 mL glass tube was charged with **1** (20.0 mg, 0.052 mmol), **2** (12.0 mg, 0.089 mmol), and a given quantity of 1,4-dioxane (0.4 ~ 2.0 mL). Then 0.2 mL of aqueous acetic acid (1 ~ 15 M) was added into the solution. The tube was flash frozen in a liquid nitrogen bath, evacuated to vacuum and flame sealed. The fused tube was then aging at room temperature for 1 to 6 days, or directly heated at different temperature (60 to 150 °C) for 3 days, or heated at 120 °C for different time of duration (0.5 to 7 days). As above-mentioned, the crude product was then isolated, post-treated and subjected to the structural identification. The phase purity of each sample was confirmed by PXRD analysis. (Note that the limit of detection of PXRD is usually 5%). The conditions we found for the controllable synthesis of COF-300 interpenetration isomers have been listed in Table S1. It can be seen that, aging (entries 14 and 15) or concentrated HOAc (entries 29 and 30) resulted in the formation of *dia-c7* COF-300; while other conditions listed in Table S1 favored the formation of *dia-c5* COF-300. As addressed in the main text, the *dia-c5* COF-300 isomer should be formed via a faster kinetic route, while the more stable *dia-c7* COF-300 isomer formed via a thermodynamic route. In this regard, adding an aging process at lower temperatures provides enough time to reach the thermodynamic equilibrium, through which the *dia-c7* COF-300 isomer was exclusively obtained. In addition, higher concentration of aqueous HOAc as the catalyst may further reduce

the energy barriers so that the thermodynamic equilibrium is reached more easily, through which the *dia-c7* COF-300 isomer can be obtained as well. According to our experimental results, the higher temperature did not benefit the crystallization of COF-300, and the crystallinity of *dia-c5* isomer obtained under 150 °C was very poor after heating for 3 days (entry 19). So we didn't use prolonging heating time at high temperature as a condition.

Table S1. Synthetic conditions for the controllable synthesis of COF-300 isomers.

Entry	Concentration of reaction mixture[a]	Aging at r.t.	Heating Temperature	Heating time	Concentration of HOAc	Product
1	**0.4 mL**	2 h	120 °C	3 d	3 M	unknown[b]
2	**0.6 mL**	2 h	120 °C	3 d	3 M	*dia-c5* COF-300
3	**0.8 mL**	2 h	120 °C	3 d	3 M	*dia-c5* COF-300
4	**1.0 mL**	2 h	120 °C	3 d	3 M	*dia-c5* COF-300
5	**1.2 mL**	2 h	120 °C	3 d	3 M	*dia-c5* COF-300
6	**1.4 mL**	2 h	120 °C	3 d	3 M	*dia-c5* COF-300
7	**1.6 mL**	2 h	120 °C	3 d	3 M	*dia-c5* COF-300
8	**1.8 mL**	2 h	120 °C	3 d	3 M	*dia-c5* COF-300
9	**2.0 mL**	2 h	120 °C	3 d	3 M	*dia-c5* COF-300
10	1.0 mL	**1 d**	120 °C	3 d	3 M	*dia-c5* COF-300
11	1.0 mL	**2 d**	120 °C	3 d	3 M	*dia-c5* COF-300
12	1.0 mL	**3 d**	120 °C	3 d	3 M	*dia-c5* COF-300
13	1.0 mL	**6 d**	120 °C	3 d	3 M	*dia-c5* COF-300
14	1.0 mL	3 d	50 °C and 120 °C	6 d	3 M	*dia-c7* COF-300
15	1.0 mL	2 h	**60 °C**	3 d	3 M	*dia-c7* COF-300[c]
16	1.0 mL	2 h	**80 °C**	3 d	3 M	*dia-c5* COF-300
17	1.0 mL	2 h	**100 °C**	3 d	3 M	*dia-c5* COF-300
18	1.0 mL	2 h	**120 °C**	3 d	3 M	*dia-c5* COF-300
19	1.0 mL	2 h	**150 °C**	3 d	3 M	*dia-c5* COF-300
20	1.0 mL	2 h	120 °C	**0.5 d**	3 M	*dia-c5* COF-300
21	1.0 mL	2 h	120 °C	**1 d**	3 M	*dia-c5* COF-300
22	1.0 mL	2 h	120 °C	**3 d**	3 M	*dia-c5* COF-300
23	1.0 mL	2 h	120 °C	**5 d**	3 M	*dia-c5* COF-300
24	1.0 mL	2 h	120 °C	**7 d**	3 M	*dia-c5* COF-300
25	1.0 mL	2 h	120 °C	3 d	**1 M**	*dia-c5* COF-300
26	1.0 mL	2 h	120 °C	3 d	**3 M**	*dia-c5* COF-300
27	1.0 mL	2 h	120 °C	3 d	**6 M**	*dia-c5* COF-300
28	1.0 mL	2 h	120 °C	3 d	**9 M**	*dia-c5* or *c7* COF-300[d]
29	1.0 mL	2 h	120 °C	3 d	**12 M**	*dia-c7* COF-300
30	1.0 mL	2 h	120 °C	3 d	**15 M**	*dia-c7* COF-300

[a] Expressed with the dosage of 1,4-dioxane.

[b] A structurally-unknown solid with undissolved monomers was obtained, the PXRD of which was different from *dia*-**c5** COF-300 or *dia*-**c7** COF-300.

[c] A solid with very poor crystallinity was obtained, the PXRD of which was similar to that of *dia-c7* COF-300.

[d] Critical condition.

B. Instrumentation

Powder X-ray diffraction (PXRD). The PXRD data of *dia-c5* and *dia-c7* COF-300 isomers were collected on a PANalytical X'Pert Pro diffractometer with the Cu Kα radiation of λ = 1.5418 Å at 40 kV and 40 mA. Prior to analysis, the samples were ground and mounted on flat sample holders. The samples were then measured with the Bragg angle (2θ) ranged from 3.0º to 50.0º with a step size of 0.013º and a scan time of 2 s per step.

Rotation Electron Diffraction (RED). The activated *dia-c7* COF-300 sample was dispersed in ethanol and treated by ultrasonication for 10 ~ 15 minutes. A droplet of the suspension was transferred onto a carbon-coated copper grid. The RED data of *dia-c7* COF-300 was collected at 200 kV using the software RED-data collection[3] with the selected-area electron diffraction (SAED) mode on a JEOL JEM2100 transmission electron microscope (TEM). During data collection, the electron beam was fully spread over the whole phosphorus screen. The selected-area aperture used for data collection was about 1 μm in diameter, which is larger than the maximum crystal size of *dia-c7* COF-300 ($< 1 \mu$m). We tracked the crystal in the image mode so as to ensure that the entire crystal was inside the aperture throughout the data collection. In total, 506 ED frames were recorded at 93 K using a cryogenic sample holder. The tilt range of the crystal sample was from $-50.82°$ to $39.00°$ with the tilt step of 0.20º. Each ED frame was recorded under the spot size 4 with the exposure time of 1 s. The total time for data collection was 45 min. The data processing was conducted with the software RED-data processing,[3] including the peak search, unit-cell determination, indexation of reflections and intensity extraction. 191 unique reflections were obtained with the resolution up to 1.65 Å. The structure of *dia-c7* COF-300 was then solved against the intensities obtained from the 3D-RED data using the simulated annealing parallel tempering algorithm implemented in the program SHELX.[4]

Solid-state nuclear magnetic resonance (SSNMR). All the SSNMR experiments were performed with magic angle spinning (MAS) on a Bruker Avance II 400 MHz wide-bore solid-state NMR spectrometer at a magnetic field of 9.4 Tesla. The ^{13}C MAS NMR data were acquired at the Larmor frequency of 100.6 MHz and the ^{13}C chemical shifts were referenced to tetramethylsilane (TMS) at 0 ppm (δ_{iso}). The ^{13}C cross-polarization (CP) MAS experiments were carried out on a standard 4 mm

double-resonance probe with the sample spinning rate of 10 kHz, with a ^{1}H $\pi/2$ pulse length of 3.2 μs, a contact time of 3 ms, a pulse delay of 3 s, and a TPPM decoupling frequency of 78.1 kHz.

N$_2$ adsorption-desorption experiments. The N$_2$ adsorption-desorption experiments were conducted on a Micromeritics ASAP 2020 Surface Area and Porosimetry Analyzer. The samples were degassed at 120 °C for 12 h before the measurements. N$_2$ isotherms were generated at 77 K by incremental exposure to high purity nitrogen up to 1 atm. Data analyses were conducted with the software ASAP 2020 V4.01.

Other characterization methods. The Fourier transform infrared (FT-IR) spectra were recorded with a Nicolet Nexus 670 FT-IR spectrometer. The thermogravimetric (TG) curves were recorded on a TA SDT Q600 simultaneous thermal analyzer, and the samples were heated with a heating rate of 10.0 °C/min from ambient temperature to 800 °C in nitrogen atmosphere. The scanning electron microscopy (SEM) images were obtained on a Hitachi S-4800 field emission scanning electron microscope at the accelerating voltages of 5.0 to 10.0 kV. The elemental analyses were carried out on an Elementar Analysensysteme GmbH vario EL cube V3.00 elemental analyzer.

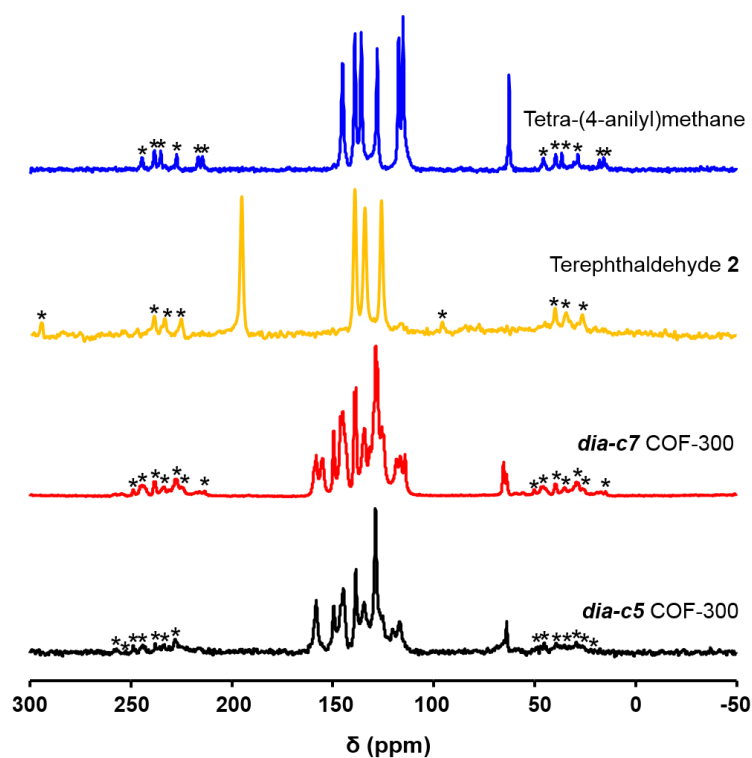## C. Solid-State Nuclear Magnetic Resonance (SSNMR) Spectroscopic Analyses

Figure S1. ^{13}C CP/MAS spectra of the monomers (**1**, blue; **2**, orange) and the COF-300 interpenetration isomers (***dia-c7***, red; ***dia-c5***, black). Asterisks denote the spinning sidebands. The ^{13}C CP/MAS NMR signals of the monomer **1** at *ca.* 190 ppm correspond to the carbon atoms at the terminal aldehyde groups (−CHO). These signals disappeared in the ^{13}C CP/MAS NMR spectra of ***dia-c5*** and ***dia-c7*** COF-300, indicating that the terminal aldehyde groups in monomer **2** have been reacted towards the construction of COF-300 framework. In addition, a new signal appears at *ca.* 158 ppm in the ^{13}C CP/MAS NMR spectra of ***dia-c5*** and ***dia-c7*** COF-300, which offers the direct evidence for the successful formation of imine bonds (−C=N−) throughout the COF-300 framework.

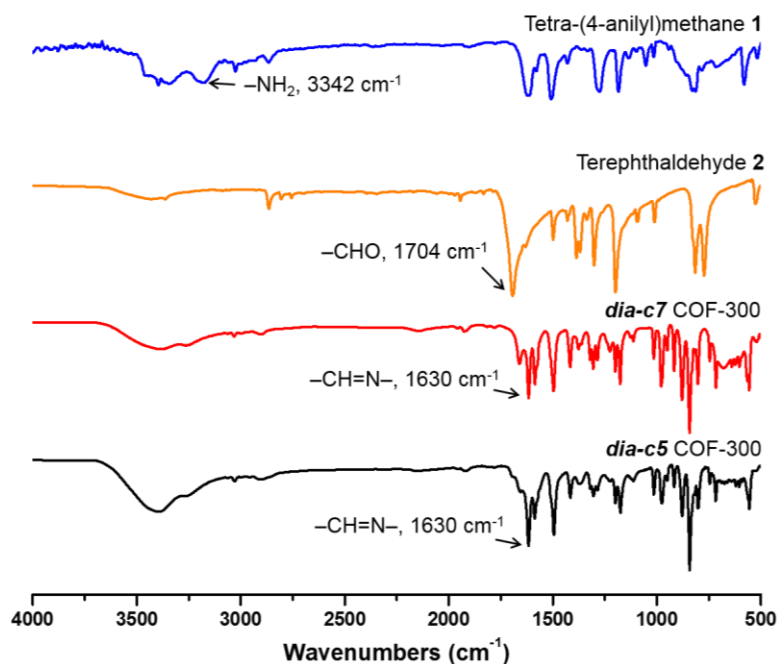# D. Fourier Transform Infrared (FT-IR) Spectroscopic Analyses

Figure S2. FT-IR spectra of the monomers (**1**, blue; **2**, orange) and the COF-300 interpenetration isomers (***dia-c7***, red; ***dia-c5***, black). The transmittance values along the Y-axis were normalized for comparison. A new $-C=N-$ stretching vibration band at 1630 and 1199 cm^{-1} in the FT-IR spectra of ***dia-c5*** and ***dia-c7*** COF-300 appears as the direct evidence for the successful formation of the imine bonds throughout the framework. Meanwhile, the weak bands at 1704 and 3342 cm^{-1} could be observed due to the existence of the terminal $-CHO$ and $-NH_2$ groups.

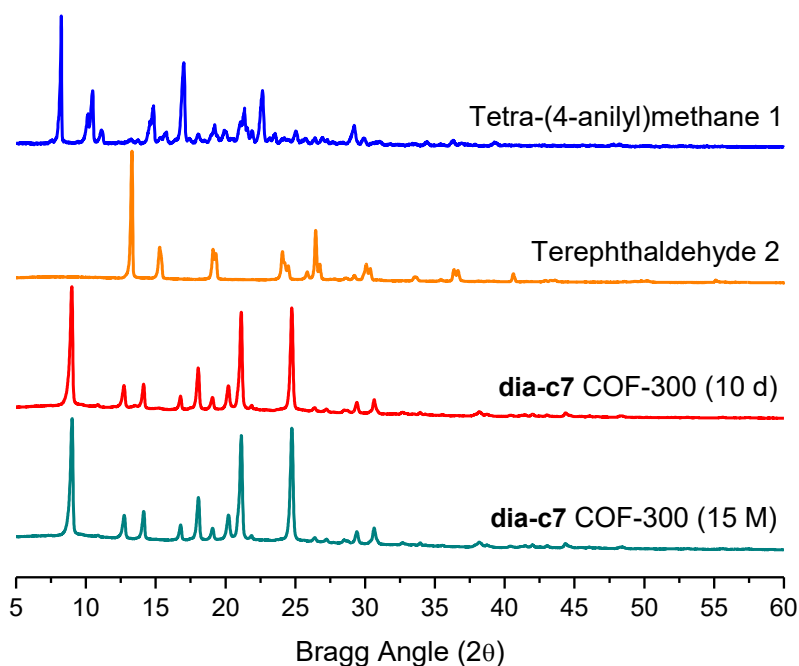# E. Powder X-ray Diffraction (PXRD) Analyses

Figure S3. PXRD patterns of the monomers (**1**, blue; **2**, orange) and *dia-c7* COF-300 synthesized in different conditions (with the duration of 10 days in total, entry 14 in Table S1, red; with 15 M of HOAc as catalyst, entry 30 in Table S1, turquoise). The intensity values along the Y-axis were normalized for comparison. The PXRD pattern of *dia-c7* COF-300 is different from those of the monomers, indicating that a new crystalline phase has been formed.
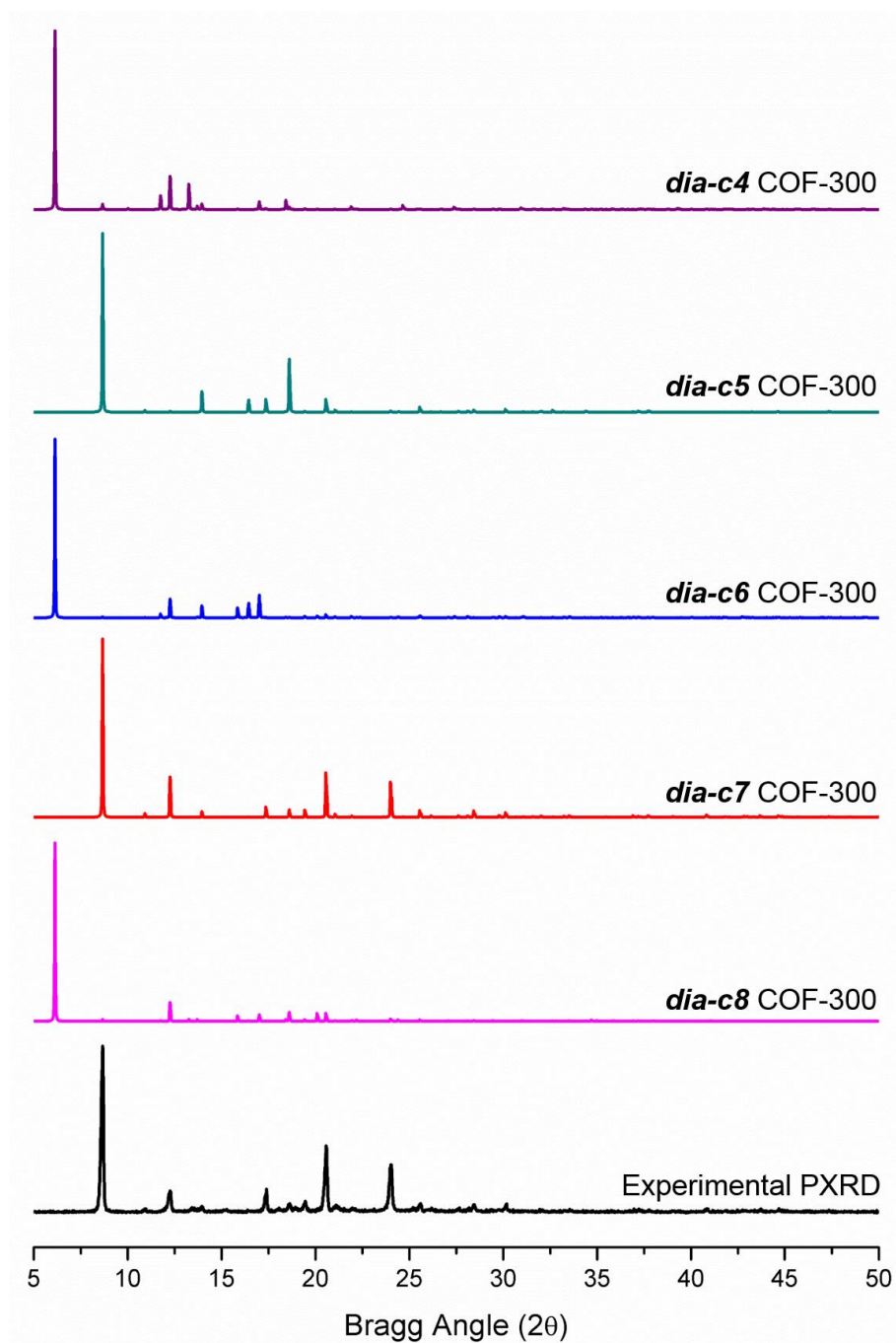
Figure S4. Simulated PXRD patterns for possible isomers of COF-300 with different interpenetration degrees from 4 to 8 (*dia-c4*, purple; *dia-c5*, turquoise; *dia-c6*, blue; *dia-c7*, red; *dia-c8*, pink). For the purpose of comparison, the experimental PXRD pattern of *dia-c7* COF-300 is shown again in black. It can be seen that only the simulated PXRD pattern with 7-fold interpenetrated structure fits well with the experimental data.

Table S2. Summary for the Rietveld refinement results of ***dia-c7*** COF-300. Detailed information for the crystal structure of ***dia-c7*** COF-300 has been included in the CIF file.

|	
Chemical formula	$C_{41}H_{28}N_4$
Formula weight	576.69
Density (calculated)/g cm^{-3}	1.0420
Crystal system	Tetragonal
Space group	$I4_1/a$
Unit cell dimensions/Å	$a = b = 20.4140(36)$, $c = 8.8216(23)$
Volume/Å^3	3676.28(4)
Z	4
Temperature/K	298(2)
X-ray source	Cu Kα
Wavelength/Å	1.5406
2θ range/°	5.000 ~ 50.000
Number of reflections	159
Number of data points	3463
Refinement method	Rietveld refinement
Rp	0.0342
Rwp	0.0465
Rexp	0.0198
GOF	2.35
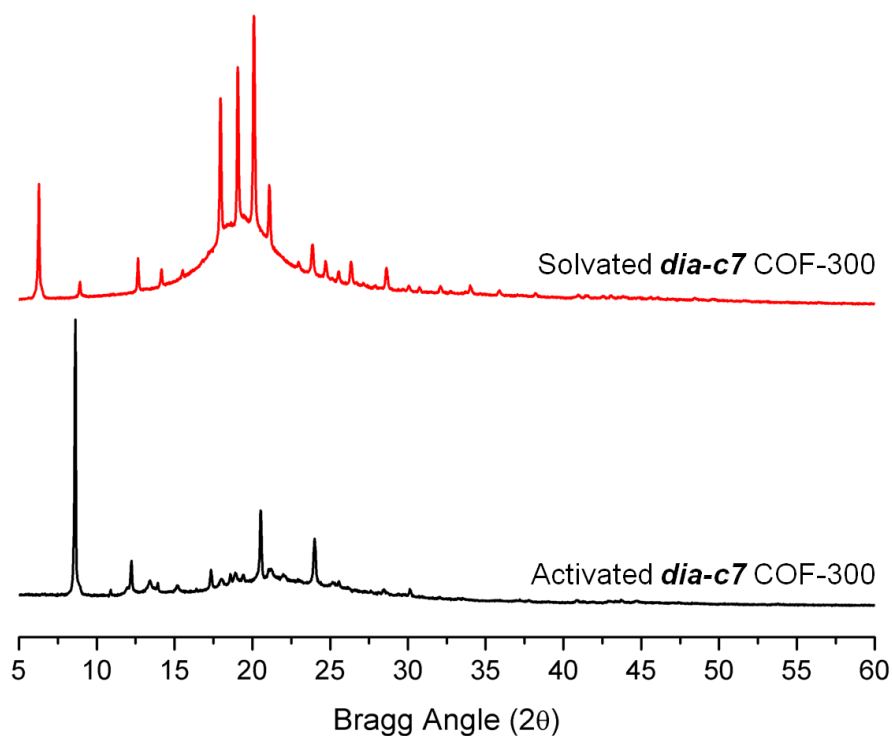
Figure S5. PXRD patterns of solvated (with 1, 4-dioxane, red) and activated (black) *dia-c7* COF-300. These PXRD data were collected on a PANalytical Empyrean diffractometer in the capillary mode with the Cu Kα radiation of $\lambda = 1.5418$ Å at 40 kV and 40 mA. The activated sample was activated at 120 °C for 12 h, and sealed in a capillary within a glove box. The solvated sample was prepared by soaking 1, 4-dioxane to the activated sample and sealed in a capillary. The data sets were collected by rotating of the corresponding capillary at a spinning rate of 0.5 r·s^{-1}. The difference in these two PXRD patterns implies the dynamic behavior[5] of *dia-c7* COF-300. This kind of "breathing" effect was also verified by N$_2$ adsorption-desorption isotherms shown in Figure S7. Note that the dynamic behavior upon guest inclusion/removal is intrinsically different[6] from the interpenetration isomerism, although both of them may cause the change of the PXRD patterns.

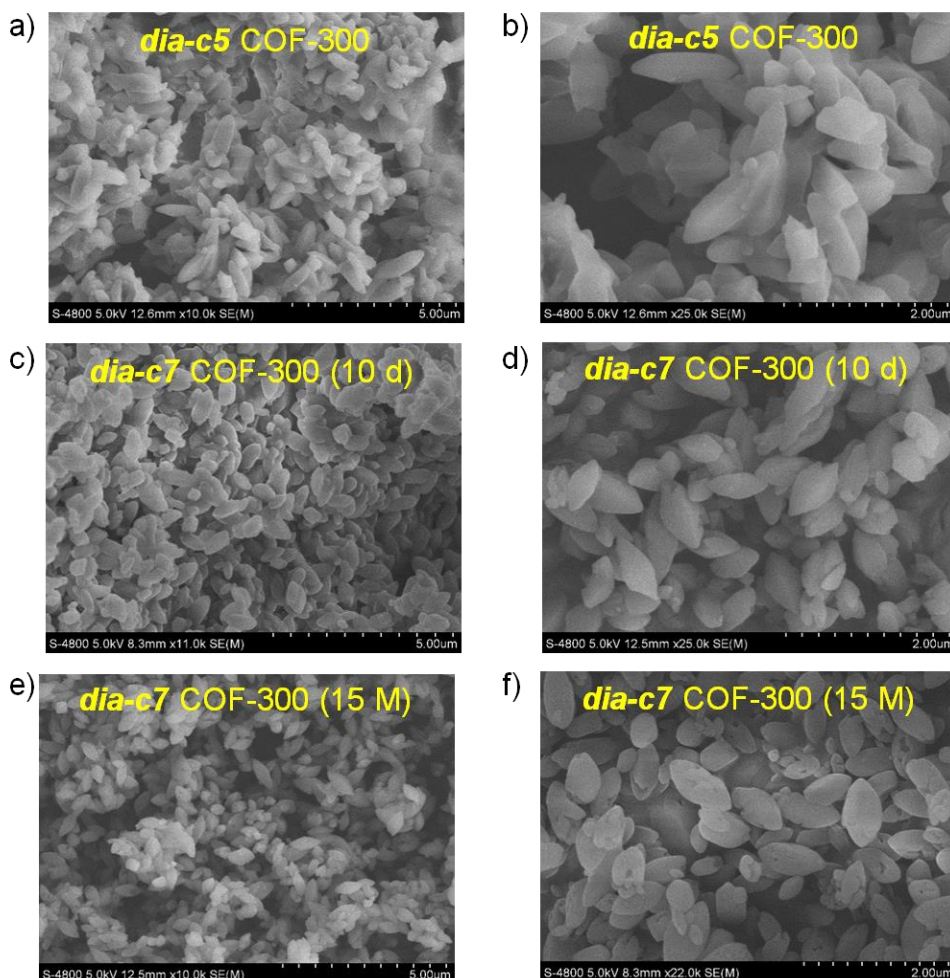# F. Scanning Electron Microscopy (SEM) Images

Figure S6. SEM images of *dia-c5* and *dia-c7* COF-300 isomers prepared in different conditions. The SEM images shown in a) and b) are those of *dia-c5* COF-300 samples synthesized according to the reported procedure[2]. The SEM images shown in c) and d) are those of *dia-c7* COF-300 synthesized with the duration of 10 days in total (entry 14 in Table S1). The SEM images shown in e) and f) are those of *dia-c7* COF-300 synthesized with 15 M of HOAc as the catalyst (entry 30 in Table S1). All the materials were obtained with well-defined and uniform morphology (grain-like shape).
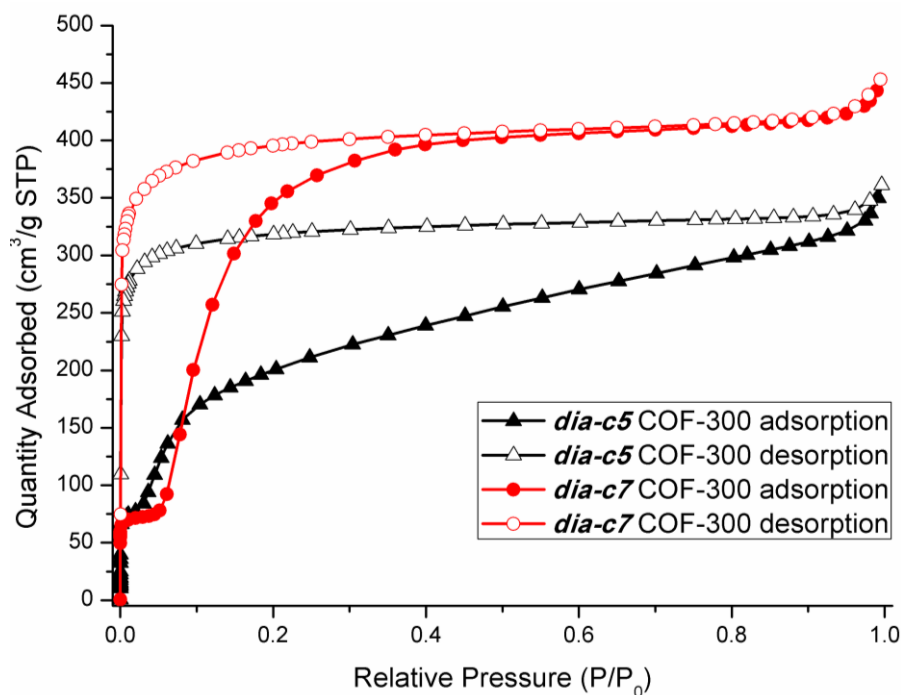
G. N$_2$ Adsorption-Desorption Experiments

Figure S7. N$_2$ adsorption-desorption isotherms of COF-300 isomers (**dia-c5**, black; **dia-c7**, red). With the hysteresis observed, the adsorption isotherm of **dia-c7** COF-300 exhibits two steps at P/P_0 = 0.0001 and 0.399 with the uptake capacities of 59.7 and 396.5 cm^3 g^{-1}, respectively. These phenomena suggested that **dia-c7** COF-300 changed its pore structure during the adsorption-desorption process, which is in accordance with the results from the PXRD analyses (Figure S5). The Brunauer-Emmett-Teller (BET) surface areas of **dia-c5** and **dia-c7** COF-300 were determined as 756 m^2 g^{-1} and 981 m^2 g^{-1} (within the range of 0.1 < P/P_0 < 0.2), respectively. The adsorption capacity for N$_2$ of **dia-c5** COF-300 is lower than that of **dia-c7** COF-300 in our experiment. However, the dynamic behavior upon guest inclusion/removal is intrinsically different in the interpenetration isomers.[6] As mentioned in the literature[2], **dia-c5** COF-300 also showed a weak dynamic response to gases (Ar used in the literature[2] and N$_2$ used in this work), but did not show here observable dynamic behaviour upon solvent inclusion/removal[2].
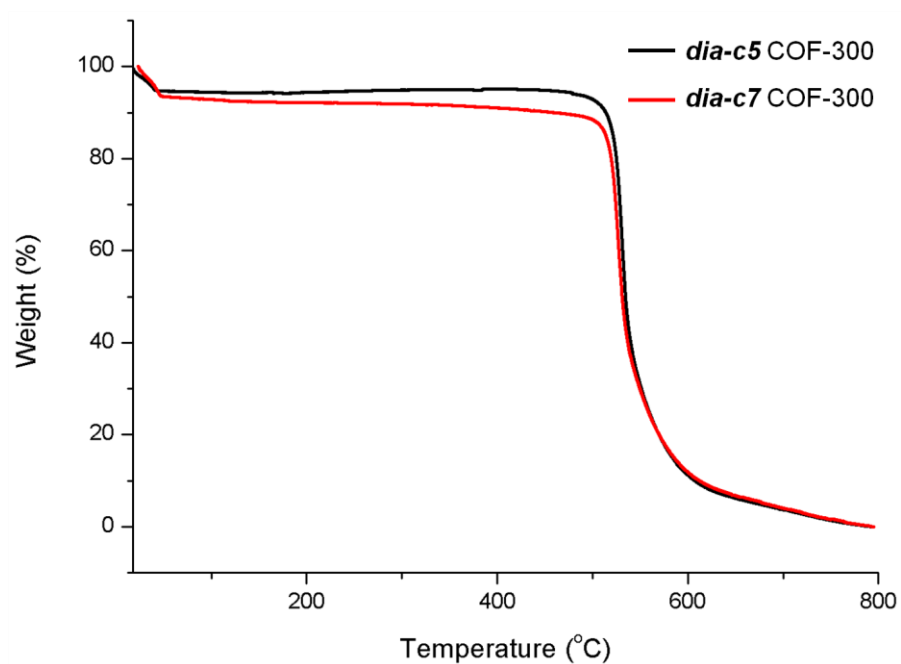
H. Thermogravimetric (TG) Analyses

Figure S8. TG curves of *dia-c5* COF-300 (black) and *dia-c7* COF-300 (red). The decomposition temperature in nitrogen is 518 $^{\circ}$C for *dia-c5* COF-300 and 521 $^{\circ}$C for *dia-c7* COF-300. Similarly, no differences in hydrothermal stability can be observed between *dia-c5* and *dia-c7* COF-300. After boiling at 100 $^{\circ}$C in water for 24 h, both of these two isomers kept their crystallinity well.

I. Formula of Interpenetration Number (*N*) in *dia*-Based Structures

General description. We develop herein a general formula to calculate the interpenetration number (*N*) for all the ***dia***-based COFs, no matter whether the tetrahedral angle (θ) in the structure is of the standard value, i.e., 109.5° (ideal case) or has been distorted to an unknown value (real cases). The formula is described as:

$$N = \frac{2\sqrt{4L^2 - a^2}}{c} \quad \text{(for } I\text{-lattice structures where } N \text{ is an odd number)}$$

or

$$N = \frac{2\sqrt{4L^2 - 2a^2}}{c} \text{ (for } P\text{-lattice structures where } N \text{ is an even number)}$$

The parameters needed for this formula are the unit cell value of *a* and *c* (which can be obtained for example from the index of the PXRD patterns), together with the length (*L*) of the organic linker (which can be given from the molecular mechanics calculation by Gaussian 09 or Material Studio 7.0). The critical derivation of the formula has been presented in detail in the following. The key trick is that we apply the intrinsic correlation between the unit cell value and *L* to replace the uncertainty brought from the distorted tetrahedral angle θ.

General relationship among the structural parameters in an interpenetrated *dia*-structure. The adamantane-like cage in any interpenetrated ***dia***-structure can be depicted in the following. The key parameters have been highlighted, which include the interpenetration number (*N*), the unit cell parameter (*c*), the length of the organic linker (*L*), and the tetrahedral angle (θ) with an unknown value.
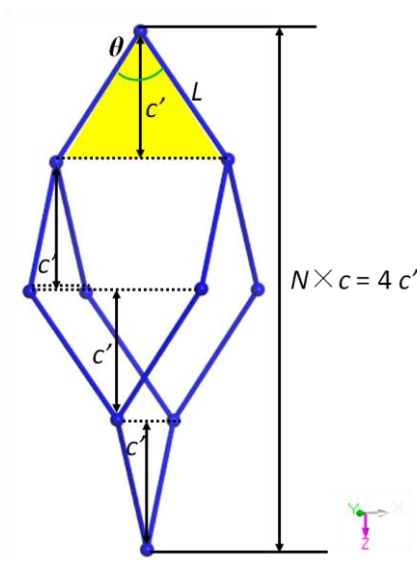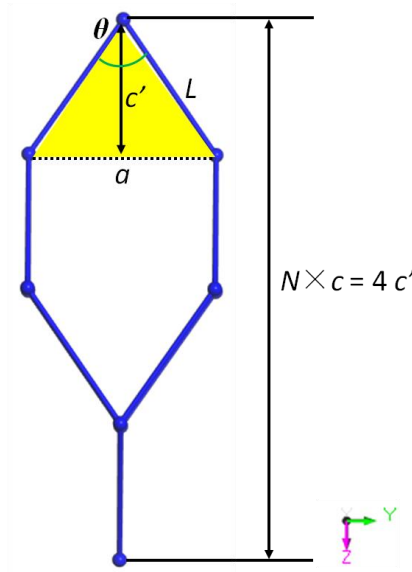
The correlation among N, c, L, and θ can be directly obtained as:

$$N \times \frac{c}{4} / L = \cos\frac{\theta}{2} \qquad\qquad (equation\ \mathbf{a})$$

Note that $c' = N \times c/4$ because any adamantane-like cage can be equally divided by 4 from the c-axis. Next, we discuss the cases of I-lattice (N is odd) and P-lattice (N is even) structures, respectively.

For the cases of I-lattice structures. The feature in an I-lattice **dia**-structure is the interpenetration with an odd number (N is odd). The key parameters in an I-lattice **dia**-structure have been depicted in the following, which include the unit cell parameters ($a = b$ and c), the length of the organic linker (L), and the tetrahedral angle (θ) with an unknown value. Viewed from the X-direction, the local structure in the odd-fold interpenetration framework is depicted as:

The correlation among a, L, and θ can be directly obtained as:

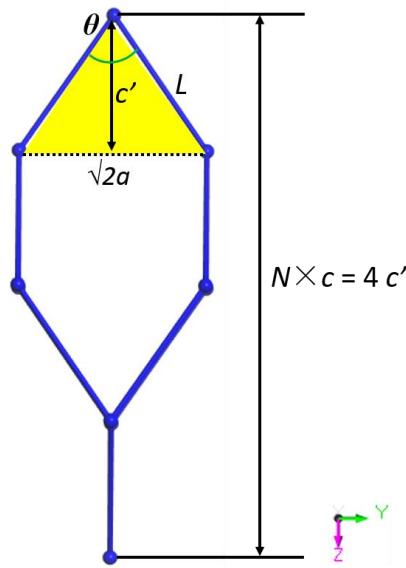$$\frac{a}{2} / L = \sin\frac{\theta}{2} \qquad\qquad (equation\ \mathbf{b1})$$

Because $\sin^2\frac{\theta}{2} + \cos^2\frac{\theta}{2} = 1$, the equations **a** and **b1** should give:

$$(\frac{a}{2L})^2 + (\frac{N \times c}{4L})^2 = 1$$

Accordingly, for the I-lattice **dia**-structures:

$$N = \frac{2\sqrt{4L^2 - a^2}}{c}, \text{ which is an odd number.}$$

For the cases of *P*-lattice structures. The feature in a *P*-lattice ***dia***-structure is the interpenetration with an even number (*N* is even). The key parameters in a *P*-lattice ***dia***-structure have been depicted in the following, which include the unit cell parameters ($a = b$ and c), the length of the organic linker (L), and the tetrahedral angle (θ) with an unknown value. Viewed from the X-direction, the local structure in the even-fold interpenetration framework is depicted as:

The correlation among a, L, and θ can be directly obtained as:

$$\frac{1}{\sqrt{2}} \times \frac{a}{L} = \sin\frac{\theta}{2} \qquad\qquad (\textit{equation } \textbf{b2})$$

Because $\sin^2\frac{\theta}{2} + \cos^2\frac{\theta}{2} = 1$, the equations **a** and **b2** should give:
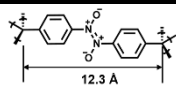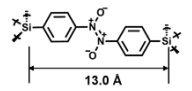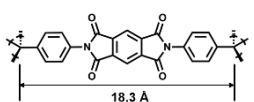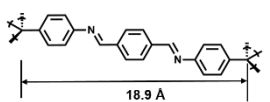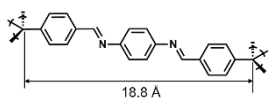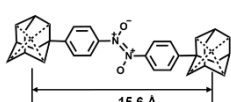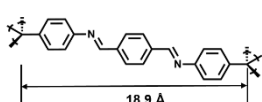
$$(\frac{1}{\sqrt{2}} \times \frac{a}{L})^2 + (\frac{c'}{L})^2 = 1$$

Accordingly, for the *P*-lattice ***dia*-**structures:

$$N = \frac{2\sqrt{4L^2 - 2a^2}}{c}, \text{ which is an even number.}$$

Table S3. Calculation for interpenetration degrees of the ***dia***-based COFs in the literature. Agreement in the degree of interpenetration (N) of 3D *dia-cN* COFs between the reported data in the literature and the calculated values from our formula:

$$N = \frac{2\sqrt{4L^2 - a^2}}{c}$$ for *I*-lattice structures (N as an odd number); $$N = \frac{2\sqrt{4L^2 - 2a^2}}{c}$$ for *P*-lattice structures (N as an even number).

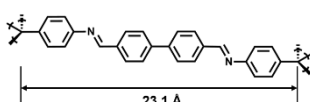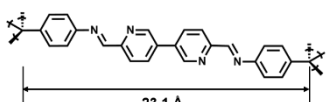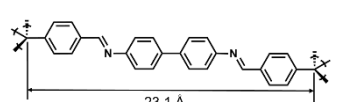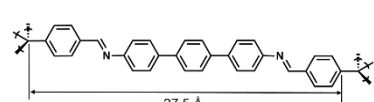| COFs[ref]	Topology[a]	$a = b$ (Å)[b]	c (Å)[b]	Space Group	L (Å)[c]	L' (Å)[d]	N[e]
NPN-1[7]	***dia-c4***	13.15	7.98	$P\text{-}4B_2$	12.3 Å	12.3	4.0 and 4.0
NPN-2[7]	***dia-c4***	13.42	8.53	$P\text{-}4B_2$	13.0 Å	12.8	4.2 and 4.0
PI-COF-5[8]	***dia-c4***	20.63	11.50	$P4/N$	18.3 Å	18.6	3.8 and 4.0
COF-300[2]	***dia-c5***	28.13	8.88	$I4_1/A$	18.9 Å	17.9	5.6[f] and 5.0
3D-IL-COF-1[9]	***dia-c5***	23.77	13.46	$I4_1/A$	18.8 Å	20.6	4.3[f] and 5.0
NPN-3[7]	***dia-c6***	15.77	7.07	$P4_2/N$	15.6 Å	15.4	6.2 and 6.0
COF-300 (*this work*)	***dia-c7***	20.41	8.82	$I4_1/A$	18.9 Å	18.5	7.2 and 7.0
COF-320[10]	***dia-c9***	30.17	7.28	$I\text{-}4_2D$	23.1 Å	22.3	9.4 and 9.0
LZU-301[5]	***dia-c9***	24.03	8.48	$I\text{-}4_2D$	23.1 Å	22.6	9.2 and 9.0
3D-IL-COF-2[9]	***dia-c9***	29.41	7.74	$I4_1/A$	23.1 Å	22.8	9.2 and 8.9
3D-IL-COF-3[9]	***dia-c11***	33.97	7.62	$I4_1/A$	27.5 Å	27.0	11.3 and 10.7

[a] The topologies reported in the original literature. [b] The unit cell data of *a*, *b*, and *c* taken from the original literature. The effective number is uniformly taken into the double digits after the decimal point. These data are available for example from the index of the corresponding PXRD pattern. [c]

The calculated length (*L*) of the organic linker (calculated herein with the Forcite module in Material Studio7.0). [d] The measured length (*L'*) of the organic linker from the crystal models reported in the original literature. [e] Every two N values are calculated from the calculated length (*L*) value and the measured length (*L'*) value, respectively. [f] Compared with **dia-c7** COF-300, the contraction of organic linker (17.9 Å) in **dia-c5** COF-300 results in a higher lattice energy which in accordance with the energy calculation results as described in the main text. And the length of organic linker between two tetrahedron nodes was stretched to 20.6 Å in a very loose structure model of 3D-IL-COF-1, it may bring in calculation deviation.

Table S4. Other interpenetrated 3D COFs. There are only 5 types of topology were reported in 3D COFs: *ctn*, *bor*, *dia* and *dia-cN*, *pts*-**c**, and *srs*-**c**. All the reported *ctn* and *bor* COFs are non-interpenetrated[11]. Nearly all the *dia*-based COFs are interpenetrated. The interpenetrated *pts-c* and *srs-c* COFs were summarized in Table S4.

COFs[ref]	Topology	Unit Cell[a]	Space Group	N[b]
3D-Py-COF[12]	*pts-c*	a = 24.41 Å	*Cmmm*	2
		b = 26.64 Å		
		c = 32.63 Å		
3D-Por-COF[13]	*pts-c*	a = 43.90 Å	$Pmc2_1$	2
		b = 23.50 Å		
		c = 21.38 Å		
SiCOF-5[14]	*srs-c*	a = 17.27 Å	*R*-3	2
SiCOF-5 (air-exposed)[14]	*srs-c*	a = 17.45 Å	*P*a-3	2

[a] The unit cell data of *a*, *b*, and *c* were taken from the original literatures. The effective number is uniformly taken into the double digits after the decimal point. [b] *N* represents interpenetration degree.

By analyzing the *pts* and *pts-c* topologies in Reticular Chemistry Structure Resource (RCSR)[15], we found that two individual *pts* nets interpenetrate to each other by translating to different axial directions with the same displacement to produce *pts-c* topology. However, in real cases such as in 3D-Por-COF[13], two individual *pts* nets interpenetrate to each other by translating to different axial directions with *different* displacement. The translation and variation in displacement will generate lots of different structures. So the calculation for interpenetration degree (*N*) in *pts-cN* structures will be difficult to be rationalized like we did in *dia-cN* structures.

By analyzing the *srs* and *srs-c* topologies in RCSR[15], we found these two structures possess the totally same unit cell and vertex. So the calculation for interpenetration degree (*N*) in *srs-cN* structures will be difficult to be rationalized like we did in *dia-cN* structures. But we can still distinguish the non-interpenetrated and interpenetrated structures by their symmetries. For example, in the ideal cases given in RCSR[15], the non-interpenetrated *srs* structure crystallizes in an *I*-lattice while the 2-fold interpenetrated *srs-c* structure crystallizes in a *P*-lattice. In the real cases, like SiCOF-5[14] as shown in Table S4, the situation may be more complicated which need to be analyzed case-by-case.

J. Energy Calculation

Table S5. Energy calculation for *dia-c5* and *dia-c7* COF-300 isomers (kcal mol^{-1}).

	dia-c5 COF-300	*dia-c7* COF-300
Total energy	-323.5	-481.8
Valence energy (diag. terms)	-356.9	-389.6
Bond	45.0	43.1
Angle	46.4	56.2
Torsion	-460.6	-495.7
Inversion	12.4	6.7
Valence energy	-67.4	-67.1
Stretch-Stretch	4.1	3.9
Stretch-Bend-Stretch	-6.0	-5.9
Stretch-Torsion-Stretch	-19.8	-19.1
Separated-Stretch-Stretch	3.3	3.1
Torsion-Stretch	-90.8	-88.2
Bend-Bend	0.0	0.0
Torsion-Bend-Bend	0.1	-0.0
Bend-Torsion-Bend	41.7	39.0
Non-bond energy	100.8	-25.0
van der Waals	88.0	-39.0
Long range correction	-2.5	-4.7
Electrostatic	15.2	18.7

The geometry optimization for *dia-c5* and *dia-c7* COF-300 isomers were calculated by the Forcite module with forcefield of COMPASS II in Material Studio 7.0. A unit cell with chemical formula of $C_{164}H_{112}N_{16}$ both in *dia-c5* and *dia-c7* COF-300 was calculated, resulting each of contribution (e.g. valence energy, bond, angle, and etc.) as shown in Table S5. The angles of tetrahedron node in *dia-c7* COF-300 are distorted more than that in *dia-c5* COF-300, which resulted more energy distribution in angle

item of 9.8 kcal/mol. However, the total energy of *dia-c7* COF-300 is lower than that of *dia-c5* COF-300 by 158.3 kcal/mol. The energy difference mainly comes from non-bond energy and van der Waals, which may be caused by more staggered benzene rings in *dia-c5* COF-300 structure than those in *dia-c7* COF-300.

K. Reference

1. (a) Grimm, M.; Kirste, B.; Kurreck, H. *Angew. Chem. Int. Ed.* **1986**, *25*, 1097-1098. (b) Ganesan, P.; Yang, X. -N; Loos, J.; Savenije, T. J. ; Abellon, R. D.; Zuilhof, H.; Sudhölter, E. J. R. *J. Am. Chem. Soc.* **2005**, *127*, 14530-14531. (c) Laliberté, D.; Maris, T.; Wuest, J. D. *Can. J. Chem.* **2004**, *82*, 386-398.

2. Uribe-Romo, F. J.; Hunt, J. R.; Furukawa, H.; Klöck, C.; O'Keeffe, M.; Yaghi, O. M. *J. Am. Chem. Soc.* **2009**, *131*, 4570-4571.

3. Wan, W.; Sun, J. -L.; Su, J.; Hovmöller, S.; Zou, X. -D. *J. Appl. Crystallogr.* **2013**, *46*, 1863-1873.

4. Sheldrick, G. *Acta Crystallgr. A* **2008**, *64*, 112-122.

5. Ma, Y. -X.; Li, Z. -J.; Wei, L.; Ding, S. -Y.; Zhang, Y. -B.; Wang, W. *J. Am. Chem. Soc.* **2017**, *139*, 4995-4998.

6. (a) Kitagawa, S.; Uemura, K. *Chem. Soc. Rev.* **2005**, *34*, 109-119. (b) Schneemann, A.; Bon, V.; Schwedler, I.; Senkovska, I.; Kaskel, S.; Fischer, R. A. *Chem. Soc. Rev.* **2014**, *43*, 6062-6096. (c) Jiang, L.; Ju, P.; Meng, X.-R.; Kuang, X.-J.; Lu, T.-B. *Sci. Rep.* **2012**, *2*, 668-672.

7. Beaudoin, D.; Maris, T.; Wuest, J. D. *Nat. Chem.* **2013,** *5*, 830-834.

8. Fang, Q.; Wang, J.; Gu, S.; Kaspar, R. B.; Zhuang, Z.; Zheng, J.; Guo, H.; Qiu, S.; Yan, Y. *J. Am. Chem. Soc.* **2015**, *137*, 8352-8355.

9. Guan, X.; Ma, Y.; Li, H.; Yusran, Y.; Xue, M.; Fang, Q.; Yan, Y.; Valtchev, V.; Qiu, S. *J. Am. Chem. Soc.* **2018**, 140, 4494–4498.

10. Zhang, Y. -B.; Su, J.; Furukawa, H.; Yun, Y.; Gandara, F.; Duong, A.; Zou, X. -D.; Yaghi, O. M. *J. Am. Chem. Soc.* **2013**, *135*, 16336-16339.

11. (a) El-Kaderi, H. M.; Hunt, J. R.; Mendoza-Cortés, J. L.; Côté, A. P.; Taylor, R. E.; O'Keeffe, M.; Yaghi, O. M. *Science* **2007**, *316*, 268-272. (b) Fang, Q.; Gu, S.; Zheng, J.; Zhuang, Z.; Qiu, S.; Yan, Y. *Angew. Chem. Int. Ed.* **2014,** *53*,

2878-2882. (c) Baldwin, L. A.; Crowe, J. W.; Pyles, D. A.; McGrier, P. L. *J. Am. Chem. Soc.* **2016,** *138*, 15134-15137.

12. Lin, G.; Ding, H.; Yuan, D.; Wang, B.; Wang C. *J. Am. Chem. Soc.* **2016**, *138*, 3302-3305.

13. Lin, G.; Ding, H.; Chen, R.; Peng, Z.; Wang, B.; Wang, C. *J. Am. Chem. Soc.* **2017**, *139*, 8705-8709.

14. Yahiaoui, O.; Fitch, N. A.; Hoffmann, F.; Fröba, M.; Thomas, A.; Roeser, J. *J. Am. Chem. Soc.* **2018**, *140*, 5330-5333.

15. O'Keeffe, M.; Peskov, M. A.; Ramsden, S. J.; Yaghi, O. M. *Acc. Chem. Res.* **2008**, *41*, 1782–1789.